

# Development of a Spherical Underwater Robot Equipped with Multiple Vectored Water-Jet-Based Thrusters

Xichuan Lin · Shuxiang Guo

Received: 27 July 2011 / Accepted: 3 January 2012  
© Springer Science+Business Media B.V. 2012

**Abstract** Research on underwater robots is attracting increased attention around the world. Various kinds of underwater robots have been developed, using an assortment of shapes, sizes, weights, and propulsion methods. In this paper, we propose a novel underwater robot, employing a spherical hull and equipped with multiple vectored water-jet-based thrusters. The overall design of the robot is first introduced, and the mechanical structure and electrical system are then individually described. Two important mechanical components are the spherical hull and the waterproof box, and these are discussed in detail. Detailed descriptions of the two-level architecture of the electrical system and the design of the water-jet thrusters are also given. The multiple vectored water-jet-based propulsion system is the key feature of the robot, and the experimental mechanism of this system is briefly explained. The three main principles behind the propulsion system are also presented. Finally, evaluation exper-

iments are presented to verify the basic motions of a prototype robot. The experimental results demonstrate that the motion characteristics of this type of underwater robot are acceptable, and the design is worthy of further research.

**Keywords** Underwater robot · Propulsion system · Water-jet thrusters · Propulsive surfaces · Basic motions · Onboard control platform

## 1 Introduction

The development of autonomous underwater robots has reached a level of practical technological maturity over the past decade. The need for autonomy in underwater robots and vehicles is becoming a prevalent issue in many situations and environments. Applications of underwater robots and vehicles have increased dramatically in recent years. Even though most autonomous underwater vehicles (AUVs) are developed for scientific underwater exploratory purposes, there are also commercial and military applications. For instance, the oil and gas industries use AUVs to make detailed maps of the seafloor before building a subsea infrastructure. AUVs allow companies to conduct precise surveys of areas where traditional bathymetric surveys would be

---

X. Lin (✉) · S. Guo  
Faculty of Engineering, Kagawa University, Kagawa,  
Japan  
e-mail: linxichuan@live.com

S. Guo  
e-mail: guo@eng.kagawa-u.ac.jp

less effective or too costly. A typical military application of an AUV is to monitor a protected area for new unidentified objects. AUVs are also employed in anti-submarine warfare, to aid in the detection of manned submarines.

Different applications or tasks require different configurations, shapes, and sizes of AUVs. For example, manipulators are necessary for mine-clearing operations and some other environmental tasks. If a robot is used for underwater environmental detection or observation, a smaller and more flexible design enables the robot to work in smaller spaces. If high-speed cruising is required, then a streamlined robot body is essential.

Design and development of autonomous underwater robots or vehicles involves different technologies, from mechanics to electronics, and from material science to hydrodynamics. Sensory, navigational, propulsion, and power systems are all essential components for underwater robots and vehicles. Typical sensors include compasses, depth sensors, side-scan and other sonar devices, magnetometers, thermistors, and conductivity probes. AUVs can navigate using an underwater acoustic positioning system. Long baseline (LBL), ultra-short baseline (USBL), or short-baseline (SBL) navigation, as well as global positioning systems (GPSs) and inertial navigation systems (INSs) are most commonly used on AUVs. The propulsion system is one of the critical factors in the performance of underwater robots, because it provides the basis for the control layers of the entire system. AUVs rely on a number of propulsion techniques, such as paddlewheels, poles, magneto-hydrodynamic drives, sails, and oars. Propeller-based thrusters are the most common by far. These thrusters are usually powered by electric motors, and sometimes rely on a lip seal to protect the internal parts of the motor from corrosion. Most AUVs in use today are powered by rechargeable batteries (lithium ion, lithium polymer, nickel metal hydride, etc.), implemented with some form of battery management system.

### 1.1 Related Work

Hundreds of different types of AUVs have been designed and developed, with varying structures

and sizes. Most of these are torpedo-like devices with streamlined bodies, as in [1]. Some are small-sized, as in [2] and [3], while others adopt various body shapes, as in [4]. Biomimetic underwater robots, which imitate the behavior of living creatures, are also an interesting area of research [5–7].

The steering strategies of traditional underwater vehicles and robots involve changing the angles of rudders or using the differential propulsive forces of two or more thrusters. However, vectored propellers are also being used on underwater vehicles and robots. Underwater vehicles with vectored thrusters are introduced in [8] and [9]. In [10], multi-channel hall-effect thrusters, which involve vector propulsion and vector composition, are discussed. An autonomous underwater vehicle equipped with a vectored thruster is proposed in [11]. The vectoring thrusters used on aircraft are also an example of a vectored propulsion system; see [12–14].

### 1.2 Motivation

The purpose of this research is to develop an underwater robot that can freely adjust its attitude by changing the direction of its propulsive forces. We would also like the robot to be flexible when moving through the water. Inspired by jet aircraft, we adopted vectored water-jet thrusters for the propulsion system. This introduced the additional requirement that all thrusters should be mounted inside the hull to protect them against collisions. A symmetrical structure would better fulfill our design objectives, and thus we considered a spherical underwater robot.

### 1.3 Structure of the Paper

In this paper, we focus on three essential issues in the development of our underwater robot. The overall design of the robot is explained in Section 2. The design and modeling of the propulsion system are then briefly described in Section 3. The results of underwater experiments are presented in Section 4 to verify the practicality of the design. Finally, conclusions and future work are discussed in Section 5.

## 2 Overall Design

Our underwater robot is spherical in shape, and equipped with a multiple vectored water-jet-based propulsion system, which differs from previous research. A type of spherical underwater vehicle with traditional blade thrusters was introduced in [15]. Watanabe [16] proposed a spherical AUV with a relatively small size and an externally installed four-blade thruster. In [17], the principles and a dynamic analysis of a new type of water-jet thruster were presented, but the system was not used on spherical underwater robots. The unmanned streamlined underwater vehicle AUV-150, developed by CMERI in India, is propelled by water-jet thrusters.

This research proposes an underwater robot with three features: spherical shape, a multiple vectored water-jet-based propulsion system, and totally internal installation. By combining the first two features, motion flexibility could be improved. Figure 1 shows the conceptual design and experimental prototype of our spherical underwater robot. The structural design of the robot was symmetric about the Z-axis. Its total diameter was 40 cm, and its weight in air was 6.3–6.5 kg.

There were two important aspects of the design that should be noted. Firstly, the robot was not bottom-heavy; the weight of the inside components was distributed. The waterproof box (containing the batteries, control boards, and other electronic components) was suspended from the top of the hull, while the thrusters were mounted in the lower part of the hull. Secondly, the Z-axis position of the waterproof box could be adjusted by four long screws. Hence, the center of mass of the robot was adjustable. Details of the mechanical structure and electrical system will be given in Sections 2.1 and 2.2.

### 2.1 Design of the Mechanical Structure

We are interested in how motion performance will be affected by using a vectored water-jet-based propulsion system on a spherical underwater robot. Therefore, we developed an experimental prototype with a minimal hardware configuration. Figure 2 shows the essential mechanical components of the robot. From left to right, these are the hull, water-jet thrusters, metal support, and waterproof box.

**Fig. 1** Overall design of the spherical underwater robot

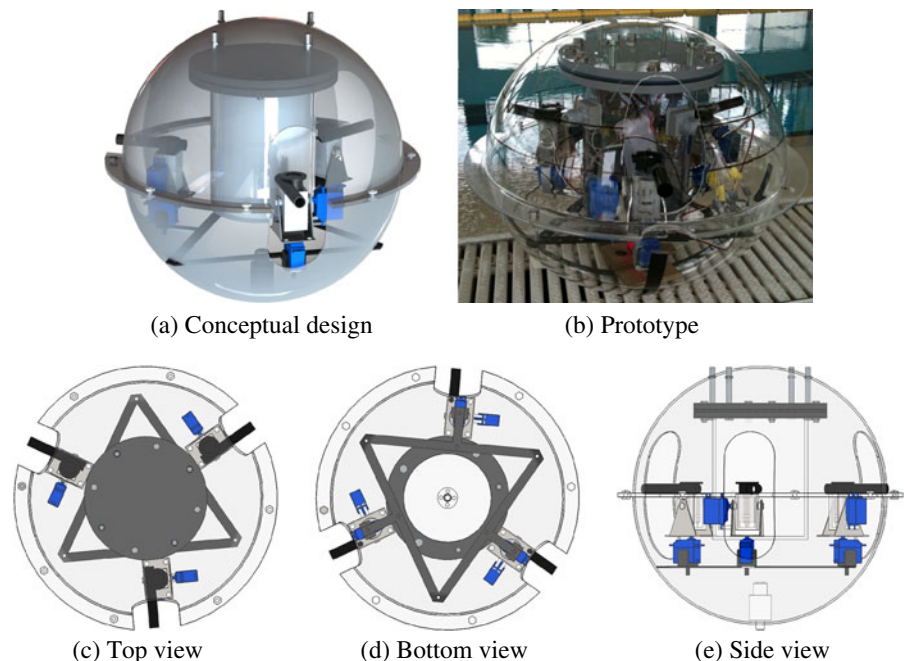
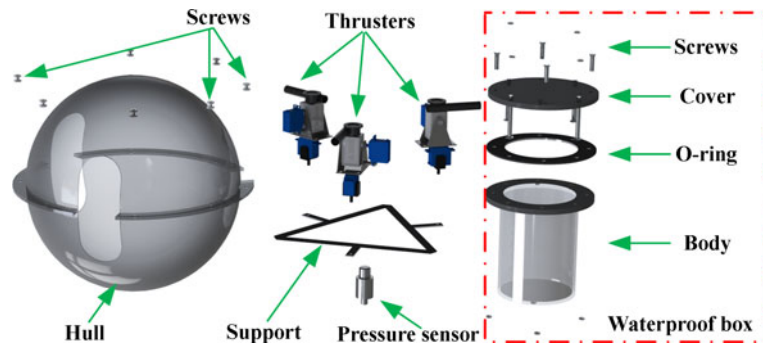


**Fig. 2** Mechanical structure of the robot



### 2.1.1 Spherical Hull

The hull is one of the most important parts of an AUV. There are various ways of designing the hull that are typically specific to the environment and task. Some essential hull design considerations are listed in [18]:

- Required pressure and/or depth
- Operating temperature range
- Impact conditions
- Visual appeal and aesthetics
- Accessibility
- Restrictions for future additions
- Size requirements

In our case, the hull was designed to bear the pressure at a water depth of at least 8 m. For the experimental prototype, the working temperature was not considered, and all experiments were carried out at room temperature (about 25–30°C). We adopted acrylic as the material for the hull. One of the advantages of using acrylic is that it is transparent, and hence optical communication devices such as cameras/phototransistors can be installed inside the hull without the use of penetrating connectors. Also, LEDs can be used to monitor the working status and other internal information without opening the hull.

The hull consisted of two hemispheres, each with a diameter of 40 cm and a thickness of 3.3 mm, as shown in Fig. 3. The connection between the hemispheres was encircled by a wing with a width of 2.5 cm for balance. Three holes were cut into the hull for the thruster nozzles. It is well known that arches and spheres are ideal structures

for pressure resistance. In this case, even though there were holes in the hull, adequate pressure resistance was provided to the robot.

### 2.1.2 Waterproof Box

Waterproofing is critical for underwater applications. Since the hull was not waterproofed, we required a waterproof box for electronic components such as batteries, control boards, and sensors. The box was also made of acrylic. Its total height was 22 cm and its inner diameter was 14 cm. As Fig. 4a and b show, there were two slots in the bottom of the box, where the control boards

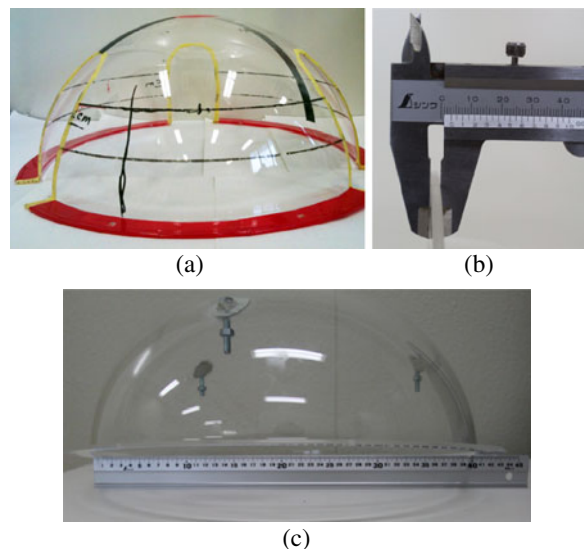
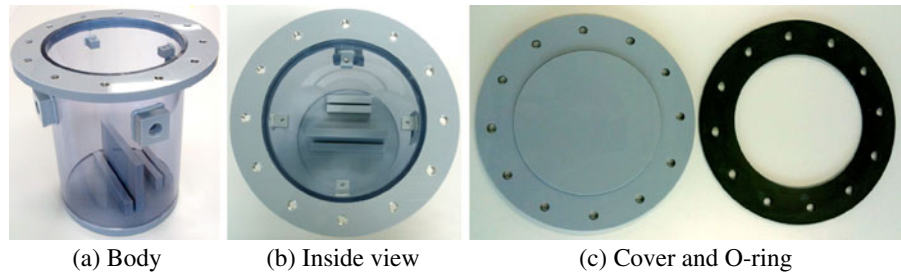


**Fig. 3** Diameter and thickness of the hull

**Fig. 4** Practical manufacturing of the waterproof box



could be attached. Figure 4c shows the cover and rubber O-ring. We used screws to seal the cover. The net weight of this box in air was 1.5 kg, and it could provide 4.4 N of buoyant force.

There were three penetrating connectors on the upper part of the box, one of which is shown in Fig. 5a. Signal cables were passed through these connectors to connect the inside control boards with the outside thrusters and pressure sensor. Figure 5b shows the SKINTOP® cable glands that we used on the box. Since they could only provide limited waterproofing capacity, it was necessary to use waterproof glue to seal the connection. Figure 5c shows a completed connection. According to tests, this box could provide waterproofing capacity at more than 15 m, which is adequate to fulfill our design requirements.

## 2.2 Design of the Electrical System

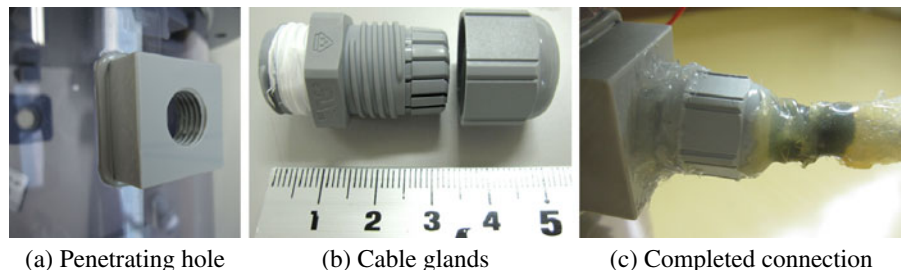
### 2.2.1 Architecture

A two-level architecture was utilized for the electrical system. Each level contained three layers. On the lower level, the bottom layer handled

all the actuators, including the servomotors and water-jet propellers. The middle layer was the driver layer, containing the motor-driving circuits. The top layer was an AVR-based control board. We used an ATmega2560 as the microprocessor unit (MPU). It could provide up to 16 MIPS of throughput at 16 MHz, which is fast enough to drive the motor and for universal asynchronous receiver/transmitter (UART) communication.

On the upper level, the bottom layer handled all the sensors (in this case, we only used one pressure sensor and one gyro sensor). The middle layer consisted of the data acquisition (DAQ) circuits. It functioned primarily as an analog to digital (AD) converter, and furnished the necessary bus conversion to the top layer. In the top layer, the main PC was an ARM module whose MPU was an ARM7TDMI core with a maximum 75 MHz of clock frequency. This PC control board had 32 MB of extended synchronous digital random-access memory (SDRAM) and 64 MB of NAND flash memory. A micro real-time operating system  $\mu$ C/OS II was embedded in the system. RS232 serial communication was used for commands and status feedback between these two levels. Fig. 6

**Fig. 5** Waterproof connection



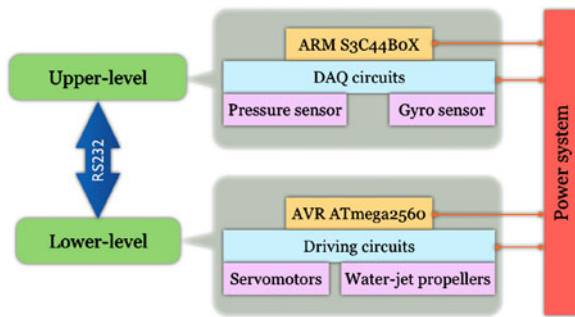
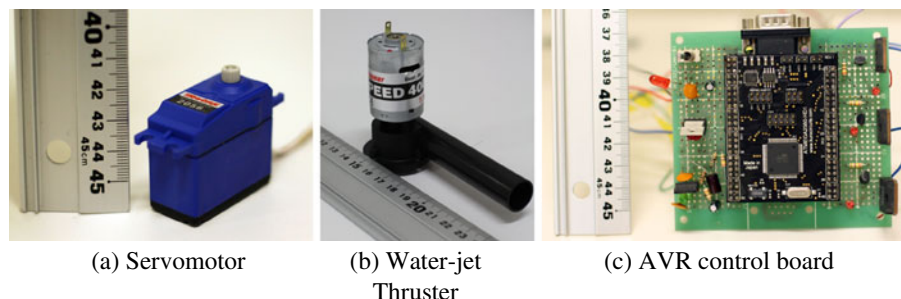


**Fig. 6** Electrical architecture of the robot

### 2.2.2 Lower Level

The lower level was the foundation of the entire system, since it included the drivers and basic components of the propulsion system. Firstly, the water-jet thrusters were equipped with TRAXXAS high-torque waterproof servos, one of which is shown in Fig. 7a. These servos provided a torque of 80 oz-in with a transit time of 0.23 s/60°. A Graupner bow thruster with an electric motor was adopted as the water-jet thruster, and is shown in Fig. 7b. It had a plastic case with a flange-mounted electric motor (SPEED 400) and an extension tube as a nozzle. The diameter of the tube was 14 mm, and the length of the tube was 60 mm. Finally, since all of the servos must be controlled separately, we needed at least 6 pulse-width modulation (PWM) channels. In addition, to control the propulsive forces of the thrusters, PWM signals were also used for propeller speed control. Therefore, a total of 9 PWM channels were necessary. The ATmega2560 provided twelve 16-bit PWM channels, which was

**Fig. 7** Lower-level components



sufficient for these controls. Another task of the ATmega2560 was receiving commands from the upper level via RS232, and converting these commands into different driving signals.

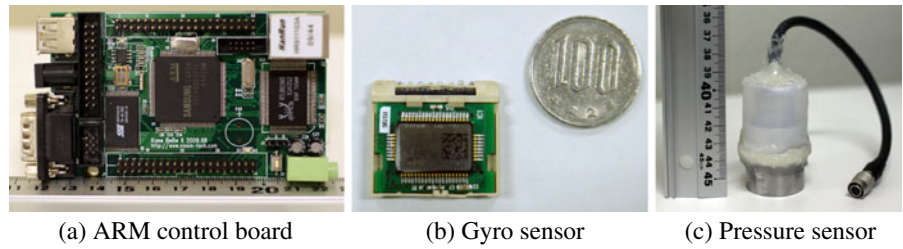
### 2.2.3 Upper Level

The upper level handled two tasks: data acquisition and the issuing of commands. Figure 8a shows the upper level control board. Firstly, the ARM obtained information from the sensors, and then performed AD conversion to prepare the data for later use. Once the digitized data were ready, they were used to calculate the actual water pressure and angular rate. These calculated values were used to describe the position and attitude of the robot. Finally, the ARM generated a series of commands that were transmitted to the lower level via RS232. The upper level continued to communicate with the lower one, not only issuing commands, but also receiving feedback from the lower level.

Figure 8b shows the gyro sensor CRS10 that was used in the experimental prototype. It was a single-axis digital angular rate sensor, manufactured using microelectromechanical systems (MEMS) technology. The sensor's primary output was accomplished via a digital serial peripheral interface (SPI) bus, providing rate information at up to 1 kHz. An analog interface was also provided for maximum flexibility, and was derived from the digital gyro information.

Figure 8c shows the XP-7001MB quartz water-pressure sensor, produced by Epon Toyocom Corporation. It had high resolution and accuracy, with a pressure measurement range of 0–100 kPa

**Fig. 8** Upper-level components

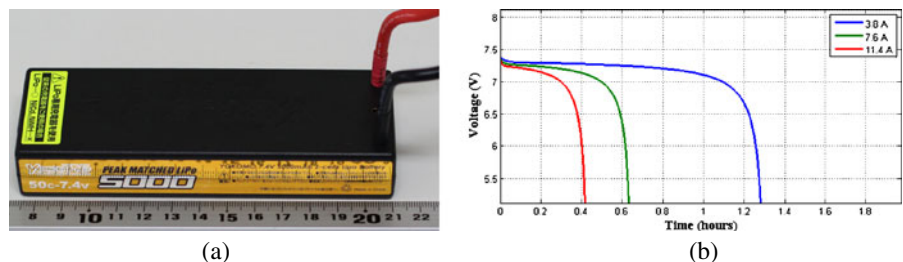


with an accuracy of  $\pm 0.05$  %FS maximum. The sensor could operate at a voltage under 6 V (DC). The RS422 bus was utilized as its data transmission mode. Its communication baud rate was set at 9600 bps with a data length of 8 bits. Because there was not an available RS422 port on the ARM control board, two MAXIM MAX485E chips were used as the converters between the RS422 and the UART port.

### 2.2.4 Power Supply

We adopted two different voltages for our spherical underwater robot. The components with the highest power consumption were the water-jet thrusters. Each of them had a working voltage of 7.2 V and a current drain of 3.5 A. The servomotors and the two control boards could operate at less than 5 V with a relatively small current. Accordingly, we used two 2-cell LiPo rechargeable batteries as the power supply for the thrusters. Figure 9a shows one of the LiPo batteries. The capacity of this battery was 5000 mAh with parameters of 50 c–7.4 V. In addition, we used 4 AA rechargeable batteries for the control boards. We carried out a power consumption test for one LiPo battery; Fig. 9b shows the battery discharge graph of the power system.

**Fig. 9** **a** One of the LiPo batteries; **b** the power discharge rate (the blue line indicates one thruster, the green line indicates two thrusters, and the red line indicates three thrusters)



## 3 Propulsion System

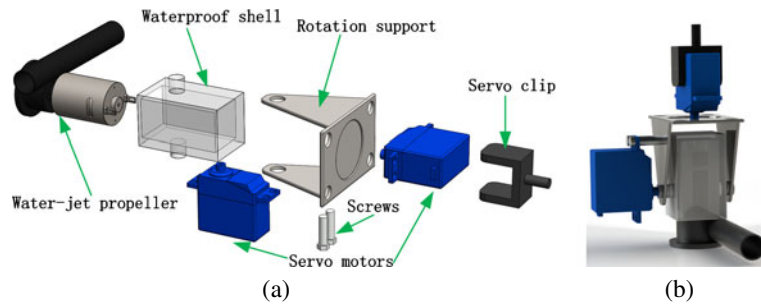
The water-jet propulsion system is the key feature of this spherical underwater robot. In the authors' previous work [19, 20] and [21], the conceptual design and modeling of the propulsion system were presented. The working principles of the water-jet thruster are discussed in [22].

### 3.1 Water-Jet Thruster Design

Figure 10 shows the design of the water-jet thruster. Its structure was simple, making it easy to assemble. It was composed of one water-jet propeller and two servomotors (above and on the side). The water-jet propeller was sealed inside a waterproof plastic box, and waterproof glue was used on the servomotors. The thruster could be rotated by the two servomotors, and hence the direction of the jetted water could be changed in the XY-plane and the XZ-plane, either respectively or simultaneously.

### 3.2 Thruster Modeling

In our previous work, we used only one strain gauge to measure the propulsive force, thereby limiting the accuracy of the model. Since a single

**Fig. 10** Structure of the water-jet thruster

strain gauge can detect force in only one direction, we considered only a 2D (horizontal plane) model. We tried to extend the model into 3D space by incorporating data from basic motion experiments. However, because of the limitations of the modeling method, the agreement between experimental and simulated results was poor. The propulsive forces and moments used in the 2D model were not correct for 3D motion. Hence, we needed to improve the methodology to obtain a more accurate model of the water-jet propulsion system.

We redesigned the experimental system so that the model could be properly constructed in 3D space. In particular, we designed a new experimental apparatus so that the mass distribution of the propulsion system was exactly the same as it is on the robot. We were primarily interested in determining the propulsive effect when the propulsion system is used on a robot, rather than simply investigating the characteristics of a single water-jet thruster. In other words, we wanted our experimental mechanism to have a propulsive effect equivalent to that of a real robot. Such a

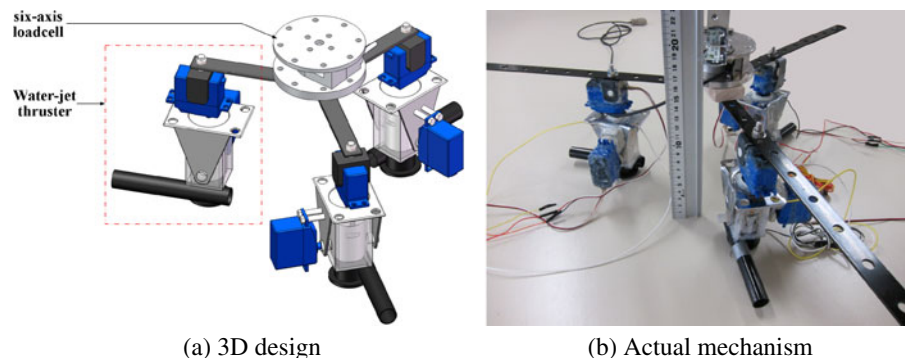
mechanism would help us to develop and improve a real propulsion system without the necessity of underwater experiments with an actual robot. The new experimental mechanism is shown in Fig. 11.

For the purpose of measuring the mean resultant force and moment in 3D space, we used a BL six-axis load cell sensor that could detect forces and torques in the X-, Y-, and Z-directions simultaneously and in real time. All the thrusters were suspended from the center of the load cell. The relative positions of the load cell and the three thrusters were the same as the relative positions of the robot center of mass and the three thrusters. In this way, we modeled the propulsion system and its propulsive effect as if it were an actual robot.

We do not include the details of the 3D modeling in this paper. Only the main principles and experimental results are presented here.

### 3.2.1 Propulsion System Coordinates

Figure 12 shows the top view of the thruster distribution. The three thrusters were mounted in a horizontal plane, circumferentially separated

**Fig. 11** Experimental mechanism design

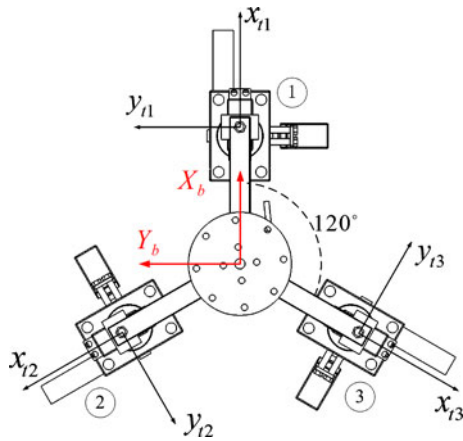


**Fig. 12** Water-jet propulsion system coordinates

from each other by an angle of  $2\pi/3$ . A thruster-fixed coordinate system was introduced, with its origin at the rotational center of the thrusters. The general transformation from thruster-fixed coordinates to robot-fixed coordinates can be written:

$${}^tP_r = \Phi_t^r \cdot {}^tP_t + C \tag{1}$$

where  ${}^tP_r$  is a vector expressed in robot-fixed coordinates,  ${}^tP_t$  is the same vector expressed in thruster-fixed coordinates,  $\Phi_t^r = (\Phi_{t1}^r, \Phi_{t2}^r, \Phi_{t3}^r)$  is the transform matrix, and  $C$  is a constant vector.

### 3.2.2 Orientation Vectors and Surface

Orientation vectors and an orientation surface are important features of the model. We defined a

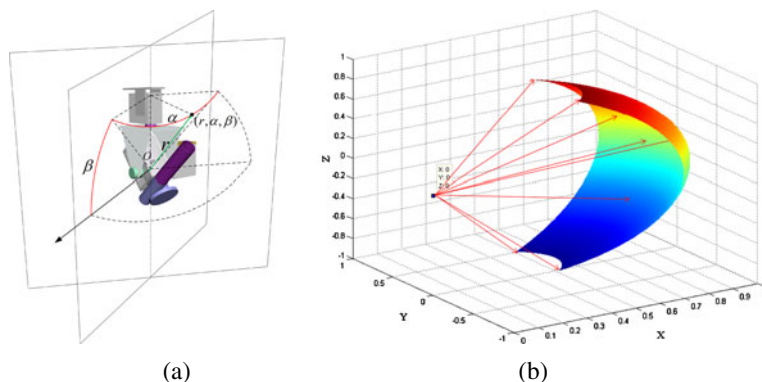
spherical coordinate system for each thruster  $P$ :  $\{r, \alpha, \beta\}$  with origin  $O_p$  at the rotational center of the thrusters, as shown in Fig. 13a. In the thruster-fixed coordinates, there were two angles that described the orientation of the nozzle: elevation and azimuth. The front end of the nozzle tracked as a spherical surface  $S_o$  whose center was at the origin of the thruster-fixed coordinates. The real orientation at each point on the surface was a normal vector to the surface, passing through the origin of the thruster-fixed coordinate system. Due to the limitations of the robot structure,  $\alpha \in [-\pi/3, \pi/3]$  and  $\beta \in [-\pi/3, \pi/3]$ . The resulting orientation vectors and surface for the water-jet thruster are shown in Fig. 13b. The normal vectors of the spherical surface can be used to determine the force vectors, and thereby used to generate the resultant mean propulsive forces. The normal vector space  $\mathbf{N} \in \mathbb{R}$  for one water-jet thruster can be written in thruster-fixed coordinates as follows:

$$\mathbf{n}_p = \left( \frac{\partial S_o}{\partial x}, \frac{\partial S_o}{\partial y}, \frac{\partial S_o}{\partial z} \right) \tag{2}$$

### 3.2.3 Propulsive Surfaces

In the experiments, varying  $\alpha$  and  $\beta$  were used as control inputs to obtain propulsive forces and moments as outputs. These variables were input in thruster-fixed coordinates, and the outputs were returned in robot-fixed coordinates. Thus, the experimental system was like a black box that included a transformation of coordinates. As a result, each thruster had different coordinate transform information. Since we were specifically

**Fig. 13** **a** Thruster-fixed coordinate system; **b** Orientation vectors and surface



focusing on combinations of different direction angles, we set the mean force of each thruster at a constant 6.5 N. For the modeling, we carried out experiments to determine the relationship between  $\alpha$  and  $\beta$  and the mean propulsive force and moment  $\tau = (F, T)$  for each thruster. Consequently, the output forces and moments were expressed as functions of  $\alpha$  and  $\beta$ . Propulsive surfaces were proposed for the purpose of describing the relationship between the input direction angles and the propulsive forces and moments. The variables  $F_x, F_y, F_z, T_x, T_y,$  and  $T_z$  can be described in the form of a third-order polynomial equation:

$$\tau(\alpha, \beta) = \sum_{i=0}^3 \sum_{j=0}^3 C_{ij} \alpha^i \beta^j \tag{3}$$

where  $C_{ij}$  is the coefficient of the term  $\alpha^i \beta^j$ .

As an example, Fig. 14 shows the experimental results and fitted surfaces for the propulsive surfaces of a single thruster. The mean resultant propulsive force and moment could be obtained by vector synthesis.

We know that, all the six variables have their own model equations which come from the general Eq. 3. To illustrate the implementation of the Eq. 3, we take the motion in horizontal plane as an example. In this case, the propulsive force should be in the horizontal plane, meanwhile, the rota-

tion moment should be minimized. Accordingly, the constrain conditions are,

$$\begin{aligned} T_z &= 0 \\ F_x &= F_{constant1} \\ F_y &= F_{constant2} \end{aligned} \tag{4}$$

where,  $F_{constant1}$  and  $F_{constant2}$  are the expected propulsive forces according to the task and the dynamics model. Then, we can solve the equations to get the angles of  $\alpha$  and  $\beta$ .

We used GPC (Generalized Predictive Control) to control the horizontal motion. In the horizontal plane, we set the control law to change the angles of  $\alpha$  and  $\beta$ , and the propulsive forces were set as constant. The control process is that the recognized CARIMA model is built at each sampling time, and accordingly, the control law will adjust to the newly recognized CARIMA model. And by carrying out the Least-squares method, the controller will calculate the necessary value of angles  $\alpha$  and  $\beta$ , according to the pre-set tracking path in horizontal plane.

#### 4 Underwater Experiments and Results for Basic Motions

It is important to evaluate the basic motions of our newly developed spherical underwater robot. Because of the symmetrical shape of the hull, it is

**Fig. 14** Propulsive surfaces of one thruster. **a** to **c** are the fitted surfaces for the forces in the x-, y-, and z-directions; **d** to **f** are the fitted surfaces for the moments in the x-, y-, and z-directions

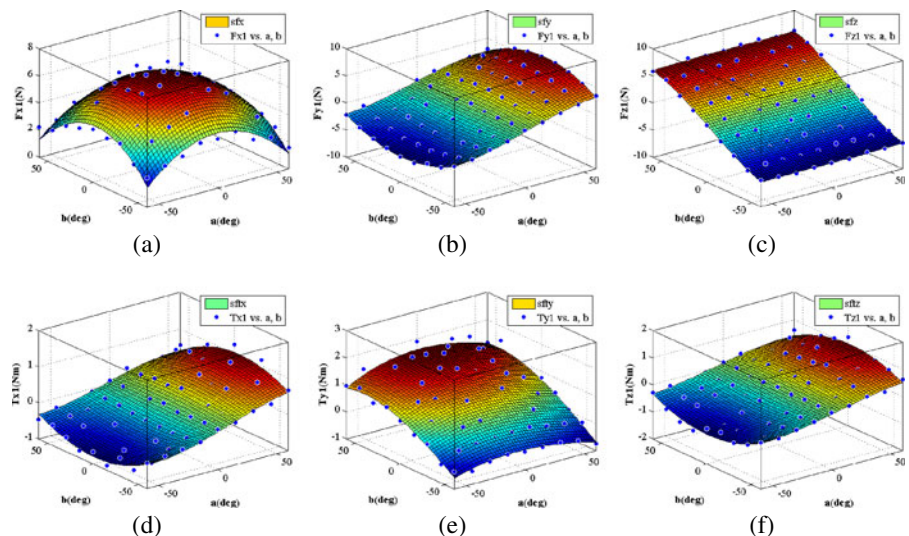
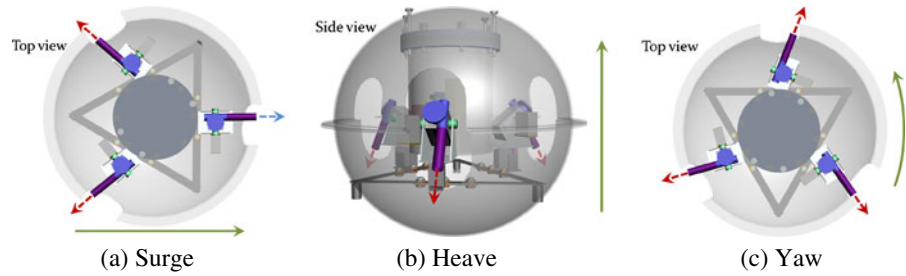


**Fig. 15** Basic motions of the experimental spherical underwater robot



obvious that the motion characteristics of surge, sway, and heave may be similar. However, from another point of view, surge and sway are motions in the XY-plane, while the motion surface of heave is perpendicular to the XY-plane. Accordingly, we carried out separate experiments for horizontal and vertical motion surfaces. Moreover, for the experimental prototype, we considered only a single rotational degree-of-freedom (DOF) about the Z-axis, and hence a third experiment on yaw motion was conducted. Figure 15 illustrates the three basic motions.

Figure 15a illustrates surge. In this case, the two water-jet thrusters on the left were used for propulsion, while the thruster on the right acted as a braking thruster to stop the robot. In the case of heave, all three water-jet thrusters worked together, and the servomotors on the sides of the thrusters all rotated through the same angle,  $\beta_i > \pi/2$  or  $\beta_i < \pi/2$ . The third case was yaw, which is rotation around the Z-axis. Expressed in thruster-fixed coordinates,  $\alpha$  should have the same orientation, clockwise or counterclockwise; i.e.,  $\alpha_i > 0$  or  $\alpha_i < 0$ . Hence, there was a rotational moment in yaw motion.

#### 4.1 Horizontal Motion Experiments

These experiments combined surge and sway to verify the motion characteristics of the ro-

bot in the horizontal plane. We carried out two experiments:

Case 1:

- Step 1: surge (move forward along the X-axis);
- Step 2: right steering (execute a 90° right turn);
- Step 3: sway (move forward along the Y-axis) (Figs. 16 and 17).

Case 2:

- Step 1: surge (move forward along the X-axis);
- Step 2: left steering (execute a 90° left turn);
- Step 3: sway (move forward along the Y-axis) (Fig. 18).

In Case 1, the timing of Step 1 was 10 s, while Step 2 took 12 s. The timings in Case 2 were close to those of Case 1, since the hydrodynamic characteristics of the right and left turns were the same. As Figs. 17 and 19 indicate, the experimental results matched the simulated results well during the surge stage, but when the robot rotated, large errors occurred. The reason for this is that we only considered linear and quadratic damping forces in the simulations, whereas in reality, there are other hydrodynamic forces acting on the robot.

#### 4.2 Vertical Motion Experiments

Although we designed the working depth of the robot to be 8 m, the depth of the experimental

**Fig. 16** Horizontal motion experiment (Case 1)

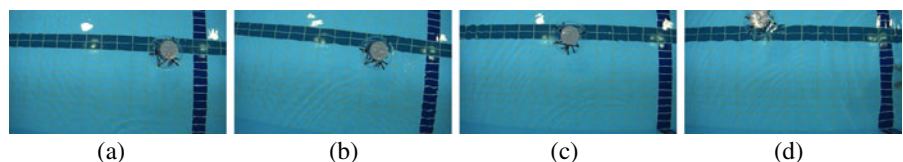
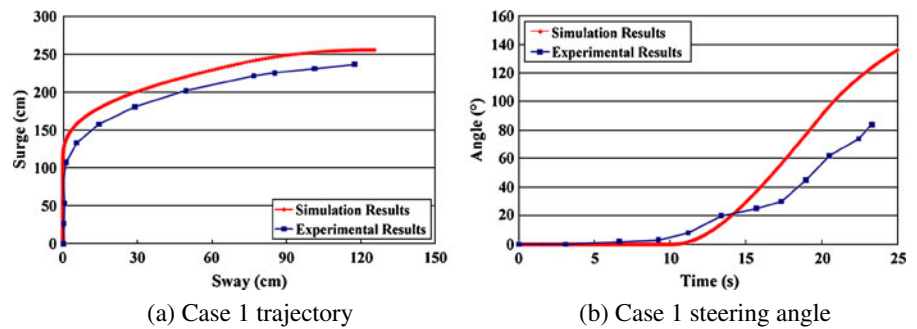


**Fig. 17** Experimental results for horizontal motion (Case 1)



pool was only 1.2 m, and hence we were only able to conduct experiments in shallow water. Accordingly, the vertical motion time was restricted to a relatively small range. We carried out two experiments:

Case 1:

- Step 1: set the topmost point of the spherical hull as the starting point;
- Step 2: move downward along the Z-axis for 7 s;
- Step 3: float upward to the water surface.

Case 2:

- Step 1: set the topmost point of the spherical hull as the starting point;
- Step 2: move downward along the Z-axis for 7 s;
- Step 3: stop the robot (Fig. 20).

As Fig. 21a and b indicate, the experimental results matched the simulated results reasonably well. The maximum errors appeared toward the top of each curve, which represents the deepest position during the experiments. When we analyzed the reasons for the errors, we found that the water pressure variation was not considered in the simulations. Also, since the control voltage to the thrusters was fixed at 7 V during the experiments, the propulsive force did not change. As a result,

the effective propulsive force was weakened by the water pressure as the depth increased.

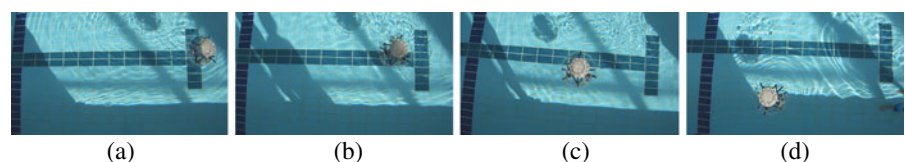
### 4.3 Yaw Motion Experiments

We ordered the robot to rotate 90° clockwise and then stop (Fig. 22). As Fig. 23a and b indicate, the maximum error between the simulated and experimental results occurred at 2.8 s, which is close to the point of maximum angular velocity. The reason for this result is that we simplified the model of our robot, especially in regard to the hydrodynamic damping forces. Only linear and quadratic damping forces were taken into account in the model. In the actual experiment, however, there were many other velocity-related hydrodynamic damping forces, and when the angular velocity increased, the damping effect of these forces ceased to be negligible.

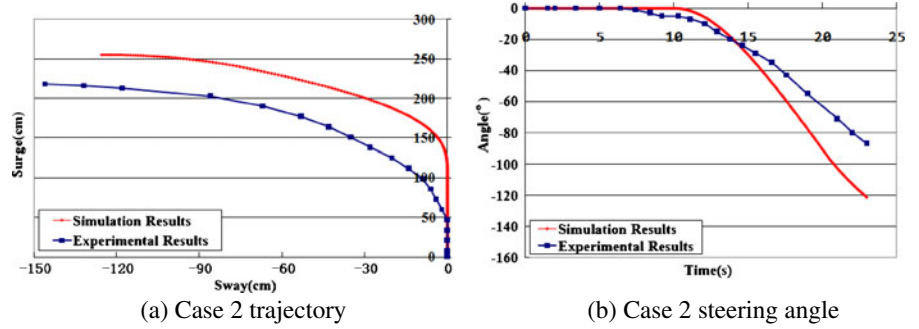
### 4.4 Discussion

All the evaluation experiments were carried out in a pool without current disturbance. Therefore, the current disturbance was not taken into account in the simulation. Meanwhile, due to that the robot is equipped with water-jet thrusters whose disturbances to the ambient water environment can be

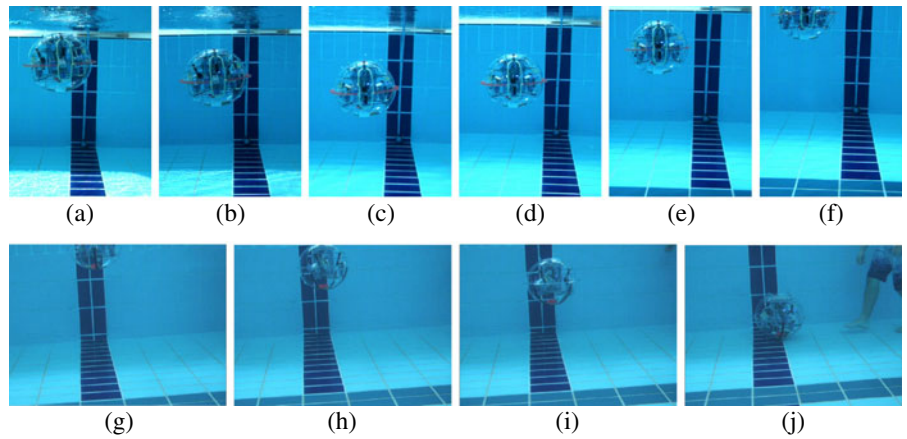
**Fig. 18** Horizontal motion experiment (Case 2)



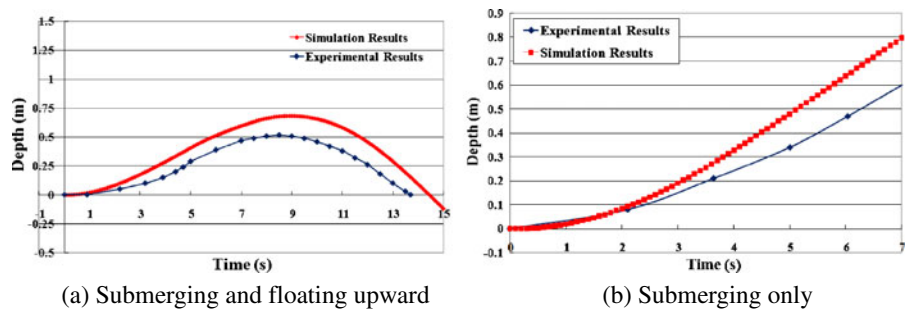
**Fig. 19** Experimental results for horizontal motion (Case 2)



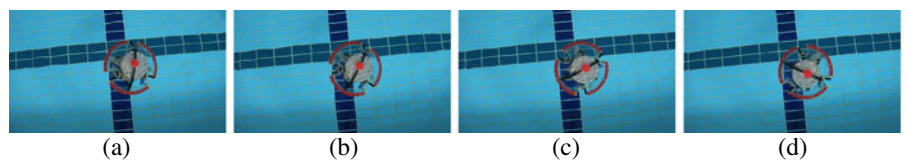
**Fig. 20** Vertical motion experiment: a to f show Case 1; g to j show Case 2

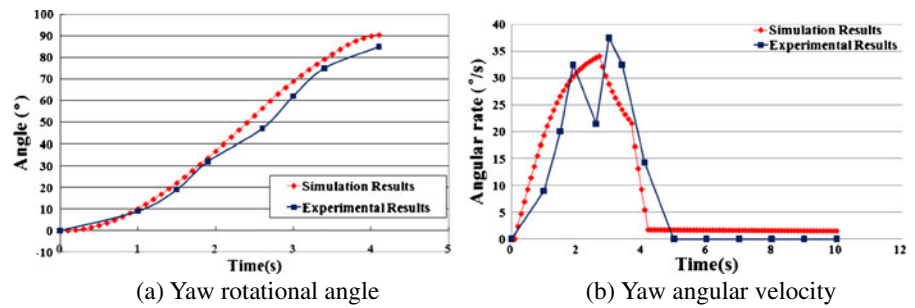


**Fig. 21** Experimental results for vertical motion



**Fig. 22** Yaw motion experiment



**Fig. 23** Experimental results for yaw motion

decreased compared with traditional screw-type thrusters.

In practical control, we must consider about the disturbances of the environment. Actually, in the experimental environment, even though no current exists, the robot may be rotated by some uncertain disturbances. If we take the surge motion as an example, the robot should move straightforward along x-axis, and two of the water-jet thrusters work for the propulsion as shown in Fig. 15a. To control this motion, we used the gyro sensor CRS10 to detect the unnecessary rotation angle in z-axis. At the initial stage, the orientation angle was set. During the surge, if the error between the detected angle and the initial one is larger than  $+10^\circ$ , which means an unnecessary rotation in clockwise, then the propulsive force of the thruster at the right side of the surge orientation will be increased to a larger amplitude to generate an added resistance torque compensating the unnecessary rotation torque. A PID controller was designed for this propulsive force adjusting. The error of orientation angle was adopted as the input of the controller, with the decreasing of the error, the increased propulsive force will fall back to its pre-set amplitude. Considering the inertia effect, the propulsive force should decrease to its pre-set amplitude in advance before the robot actually rotates back to the right direction. The amount of advance was set to 30% of the error angle.

## 5 Conclusions and Future Work

In this paper, we proposed a spherical underwater robot employing three vectored water-jet

thrusters as its propulsion system. We discussed the design details of the mechanical structure and the electrical system. The mechanical design was simple and modulated, making it easy to assemble the robot. A two-level architecture was utilized for the electrical system, and this was described in detail. A brief description of the water-jet thruster design was also provided. Then the three main principles of the vectored water-jet propulsion system were explained, namely the propulsion system coordinates, the orientation vectors and surface, and the propulsive surfaces. These three principles contained the basic concepts of this propulsion system.

An experimental prototype was developed for the purpose of basic motion evaluation, and underwater experiments were carried out. Surge, heave, and yaw were separately investigated to verify the basic motions. The results of each experiment were presented, and error sources were discussed, which is important for the next step in the development and improvement of the robot.

The underwater experiments with the prototype robot demonstrated the practicality of the design, indicating that the water-jet propulsion system worked well for different motions. However, there were also some problems that need to be resolved. Firstly, the propulsive forces of the water-jet thrusters must be increased. Secondly, the effect of water pressure variation on the propulsive forces should be considered when constructing a dynamical model of the thrusters. Thirdly, the mass distribution should be reconfigured to improve stability. Finally, the experiments showed that it is necessary to improve the accuracy of the dynamical model of the robot to achieve precise control.

**Acknowledgement** This research was supported by the Kagawa University Characteristic Prior Research Fund 2011.

The English in this document has been checked by at least two professional editors, both native speakers of English. For a certificate, please see: <http://www.textcheck.com/certificate/8PLsqH>.

## References

1. Sangekar, M., Chitre, M., Koay, T.: Hardware Architecture for a Modular Autonomous Underwater Vehicle STARFISH. In: IEEE OCEANS 2008, pp. 1–8 (2009)
2. Allen, B., Stokey, R., Austin, T., Forrester, N., Goldsborough, R., Purcell, M. von Alt, C.: REMUS: a small, low cost AUV; system description, field trials and performance results. In: OCEANS'97, MTS/IEEE Conference Proceedings, vol. 2, pp. 994–1000 (2002)
3. Madhan, R., Desa, E., Prabhudesai, S., Sebastiao, L., Pascoal, A., Desa, E., Mascarenhas, A., Maurya, P., Navelkar, G., Afzulpurkar, S., et al.: Mechanical design and development aspects of a small AUV-Maya. In: 7th IFAC Conference MCMC2006 (2006)
4. Antonelli, G., Chiaverini, S.: Adaptive tracking control of underwater vehicle-manipulator systems. In: Proceedings of the 1998 IEEE International Conference on Control Applications, vol. 2, pp. 1089–1093 (2002)
5. Menozzi, A., Leinhos, H.A., Beal, D.N., Bandyopadhyay, P.R.: Open-loop control of a multifin biorobotic rigid underwater vehicle. IEEE J. Oceanic Eng. **33**(2), 112–116 (2008)
6. Gao, B., Guo, S., Ye, X.: Motion-control analysis of ICPF-actuated underwater biomimetic microrobots. International Journal of Mechatronics and Automation **1**(2), 79–89 (2011)
7. Pan, Q., Guo S., Okada T.: A novel hybrid wireless microrobot. International Journal of Mechatronics and Automation **1**(1), 60–69 (2011)
8. Cavallo, E., Michelini, R., Filaretov, V.: Conceptual design of an AUV equipped with a three degrees of freedom vectored thruster. J. Intell. Robot. Syst. **39**(4), 365–391 (2004)
9. Le Page, Y., Holappa, K.: Hydrodynamics of an autonomous underwater vehicle equipped with a vectored thruster. In: IEEE OCEANS2000 MTS/IEEE Conference and Exhibition, vol. 3, pp. 2135–2140 (2002)
10. Duchemin, O., Lorand, A., Notarianni, M., Valentian, D., Chesta, E.: Multi-channel hall-effect thrusters: mission applications and architecture trade-offs. In: 30th International Electric Propulsion Conference (2007)
11. Le Page, Y., Holappa, K.: Simulation and control of an autonomous underwater vehicle equipped with a vectored thruster. In: IEEE OCEANS2000 MTS/IEEE Conference and Exhibition, vol. 3, pp. 2129–2134. (2002)
12. Kowal, H.: Advances in thrust vectoring and the application of flow-control technology. Journal of Canadian Aeronautics and Space **48**(2), 145–151 (2002)
13. Beal, B.: Clustering of Hall Effect Thrusters for High-Power Electric Propulsion Applications. The University of Michigan (2004)
14. Lasic, D., Ristanovic, M.: Electrohydraulic thrust vector control of twin rocket engines with position feedback via angular transducers. Control Eng. Pract. **15**(5), 583–594 (2007)
15. Do, K.D., Jiang, Z.P., Pan, J., Nijmeijer, H.: A global output-feedback controller for stabilization and tracking of underactuated ODIN: a spherical underwater vehicle. Automatica **40**(1), 117–124 (2004)
16. Watanabe, K.: An AUV based experimental system for the underwater technology education. In: OCEANS 2006-Asia Pacific, pp. 1–7 (2006)
17. Yang, P., Zhang, C., Zhang, S.: Operational principle and dynamic analysis of a new-type water-jet propeller. Journal of Lanzhou University of Technology **3** (2009)
18. Wang, W.H., Engelaar, R.C., Chen, X.Q., Chase, J.G.: The state-of-art of underwater vehicles-theories and applications. Mobile Robots, I-Tech Education and Publishing (2009)
19. Guo, S., Lin, X., Hata, S.: A conceptual design of vectored water-jet propulsion system. In: Proceedings of the 2009 IEEE International Conference on Mechatronics and Automation, pp. 1190–1195 (2009)
20. Guo, S., Lin, X., Tanaka, K., Hata, S.: Modeling of water-jet propeller for underwater vehicles. In: Proceedings of the 2010 IEEE International Conference on Automation and Logistics, pp. 92–97 (2010)
21. Lin, X., Guo, S., Tanaka, K., Hata, S.: Development and evaluation of a vectored water-jet-based spherical underwater vehicle. INFORMATION: An International Interdisciplinary Journal **13**(6), 1985–1998 (2010)
22. Guo, S., Lin, X., Tanaka, K., Hata S.: Development and control of a vectored water-jet-based spherical underwater vehicle. In: Proceedings of the 2010 IEEE International Conference on Information and Automation, pp. 1341–1346 (2010)